Constraint on the cosmological $f(R)$ model from the multipole power spectrum of the SDSS luminous red galaxy sample and prospects for a future redshift survey

Kazuhiro Yamamoto,[1,*] Gen Nakamura,[1,†] Gert Hütsi,[2,‡] Tatsuya Narikawa,[1,§] and Takahiro Sato[1,‖]

[1]*Department of Physical Science, Hiroshima University, Higashi-Hiroshima 739-8526, Japan*

[2]*Tartu Observatory, EE-61602 Tõrevere, Estonia*

(Received 30 December 2009; published 13 May 2010)

A constraint on the viable $f(R)$ model is investigated by confronting theoretical predictions with the multipole power spectrum of the luminous red galaxy sample of the Sloan Digital Sky Survey, data release 7. We obtain a constraint on the Compton wavelength parameter of the $f(R)$ model on the scales of cosmological large-scale structure. A prospect of constraining the Compton wavelength parameter with a future redshift survey is also investigated. The usefulness of the redshift-space distortion for testing the gravity theory on cosmological scales is demonstrated.

DOI: 10.1103/PhysRevD.81.103517 PACS numbers: 98.80.−k, 95.30.Sf, 95.36.+x, 98.80.Es

I. INTRODUCTION

Experimental tests of gravity on the scale of the Solar System show good agreement with predictions of general relativity (e.g., [1]). The nature of the Newtonian gravity is the attractive force, which naturally predicts a decelerated expansion of the Universe. Contrary to this expectation, it has been discovered that our Universe is undergoing an accelerated expansion epoch [2–4]. Though the accelerated expansion is explained by introducing a cosmological constant, its small but nonzero value cannot be explained naturally [5]. The problem might be deeply rooted in the nature of fundamental physics.

This problem has attracted many researchers, and many works have been done, both theoretically and observationally. As a generalization of the cosmological constant, dynamical fields, called the dark energy model and its variants, are proposed to explain the accelerated expansion of the Universe (see [6] and references therein). As an alternative to the dark energy model, modification of gravity may explain the accelerated expansion. General relativity is not considered to be the complete theory, because its quantum theory cannot be formulated in a well defined manner. The theory of gravity might need to be reformulated within a more general framework.

From the observational point of view, the constraint on the gravity theory on cosmological scales has not been well investigated, compared with the constraint on the scales of the Solar System. Many future projects to produce large galaxy surveys are in progress or planned [7–12], which aim to explore the nature of the dark energy. These surveys are useful for testing the theory of gravity at cosmological scales (e.g., [13]). The dynamical dark energy models may have similar expansion rates as models of modified gravity, but predict different histories for the growth of structures. The key to testing the gravity theory is the measurement of the evolution of cosmological perturbations, as many authors have concluded recently [14–25].

The cosmic microwave background (CMB) anisotropies are useful for investigating the cosmological perturbations through the measurements of the integrated Sachs-Wolfe effect or the lensing effect on the angular power spectrum [26]. Imaging surveys of galaxies are also useful through the weak lensing statistics or cluster number counts [27,28]. Similarly, redshift surveys of galaxies are helpful for testing gravity [29–34]. In the present paper, we revisit the problem of testing the gravity theory through a measurement of the multipole power spectra in the Sloan Digital Sky Survey (SDSS) luminous red galaxy (LRG) sample [31]. Measuring the multipole power spectra is a way to estimate the redshift-space distortions, which reflect the linear growth rate of the matter density perturbations [35–37].

Many authors have investigated the clustering nature of the SDSS LRG sample [38–47]. In Refs. [48,49], recent results on LRGs from the SDSS data release (DR) 7 are reported. In Ref. [46], a test of gravity is considered using the observed anisotropic correlation function. Three of the authors of the present paper have shown that the SDSS LRG sample is useful to test the gravity theory by measuring the quadrupole power spectrum of galaxy distribution, which represents the redshift-space distortions [31]. In the present paper, we revisit the issue of testing the gravity theories on cosmological scales using the SDSS LRG sample of DR 7, especially focusing on the $f(R)$ gravity model.

The $f(R)$ models proposed in [50–53] are viable models of modified gravity, which include some function of the Ricci scalar $f(R)$ added to the Einstein-Hilbert action. As the modification of gravity involves the introduction of an extra degree of freedom in general, one must be careful with the resulting behavior. Furthermore, any theory must reduce to the general relativity on the scales of the Solar

*kazuhiro@hiroshima-u.ac.jp
†gen@theo.phys.sci.hiroshima-u.ac.jp
‡gert@aai.ee
§narikawa@theo.phys.sci.hiroshima-u.ac.jp
‖sato@theo.phys.sci.hiroshima-u.ac.jp

System. In the $f(R)$ model, the general relativity is supposed to be recovered by the *chameleon mechanism* [54,55], which hides the field of the extra degree of freedom because the mass of the field becomes large for a dense region. The cosmological bounds on the $f(R)$ model have been investigated with the cosmic microwave background anisotropies [56] and also using the abundance of galaxy clusters [57]. However, our approach is based on the redshift-space distortion [58].

This paper is organized as follows. In Sec. II, we briefly review the $f(R)$ model and the characteristic evolution of the matter density perturbation. In Sec. III, we present our results for the multipole power spectrum of the SDSS LRG sample of the DR 7. In Sec. IV, the cosmological constraint is discussed by confronting the observed multipole spectra with the theoretical predictions. In Sec. V, a prospect of constraining the $f(R)$ model is discussed on the basis of the Fisher matrix analysis, assuming a future large redshift survey. Section VI is devoted to summary and conclusions. Throughout this paper, we use units in which the velocity of light equals 1, and adopt the Hubble parameter $H_0 = 100h$ km/s/Mpc with $h = 0.7$.

II. $f(R)$ GRAVITY MODEL

In this section, we briefly review the $f(R)$ model, proposed in Refs. [50–53]. In general, higher derivative terms are expected in the low-energy effective action of gravity. Inspired by this, the $f(R)$ model introduces some function of the Ricci scalar $f(R)$, adding to the Einstein-Hilbert action. We consider the theory defined by

$$S = \frac{1}{16\pi G}\int d^4x\sqrt{-g}(R + f(R)) + S_m, \tag{1}$$

where S_m is the action of the matter. Many aspects of the $f(R)$ model have been investigated; see e.g. [60,61] for a review (cf. [62,63]). We assume that the chameleon mechanism is responsible for the recovery of the general relativity on Solar-System scales. The chameleon mechanism is a nonlinear effect. Recently, the effect on the quasinonlinear power spectrum was investigated based on the perturbative approach or the numerical simulations [64–67]. This nonlinear chameleon effect becomes influential in the nonlinear regime. In the present paper, however, we can neglect the nonlinear chameleon effect because we need to consider only rather large scales, $k \lesssim 0.2h$ Mpc^{-1}.

For the viable model, the function $f(R)$ must satisfy some conditions. We consider the model where the asymptotic form of $f(R)$ can be expressed by

$$f(R) \simeq -2\Lambda\left[1 - \left(\frac{R_c}{R}\right)^{2n}\right], \tag{2}$$

where Λ is the cosmological constant, n is a constant that specifies the $f(R)$ model, and R_c is also a constant with the same dimension as that of the Ricci scalar. The background expansion of this $f(R)$ model is well approximated by that of the ΛCDM model.

It is known that the additional term $f(R)$ involves the introduction of an extra degree of freedom. Namely, $f_R \equiv df/dR$ corresponds to the extra degree of freedom, which behaves like a scalar field. From the above action, one can derive the equation for f_R,

$$\nabla_\mu\nabla^\mu f_R = \frac{1}{3}(R + 2f - Rf_R) + \frac{8\pi G}{3}(-\rho + 3P), \tag{3}$$

where ρ and P are the energy density and the pressure of the matter, respectively. If we regard the right-hand side of Eq. (3) as the derivative of the effective potential $dV_{\rm eff}/df_R$, the mass of f_R can be read

$$m^2 = \frac{d^2V_{\rm eff}}{df_R^2} = \frac{1}{3}\left(\frac{1 + f_R}{f_{RR}} - R\right). \tag{4}$$

The viable $f(R)$ theory satisfies $f \ll R$, and $|f_R| \ll 1$. Assuming $Rf_{RR} \ll 1$, the mass of the extra degree of freedom is

$$m^2 \simeq \frac{1}{3}\frac{1}{f_{RR}}, \tag{5}$$

where $f_{RR} = d^2f/dR^2$. Thus, $f_{RR} > 0$ is required to avoid the extra degree of freedom becoming tachyonic. This extra degree of freedom mediates an attractive force, and modifies the gravity from the range determined by the Compton wavelength $\lambda = 1/m$. From Eq. (2), we have

$$f_{RR} = \frac{d^2f(R)}{dR^2} = 4n(2n + 1)\Lambda\frac{R_c^{2n}}{R^{2n+2}}. \tag{6}$$

In the subhorizon limit, the matter density perturbation follows (e.g., [68] and references therein),

$$\ddot{\delta} + 2\frac{\dot{a}}{a}\dot{\delta} - 4\pi G_{\rm eff}(a, k)\rho\delta = 0, \tag{7}$$

where

$$\frac{G_{\rm eff}(a, k)}{G} = 1 + \frac{1}{3}\frac{k^2/a^2}{k^2/a^2 + 1/(3f_{RR})}, \tag{8}$$

and the dot denotes the differentiation with respect to the cosmic time.

Instead of R_c, we introduce the parameter k_c by

$$\frac{1}{3f_{RR}} = k_c^2\left(\frac{\Omega_0/a^3 + 4(1 - \Omega_0)}{\Omega_0 + 4(1 - \Omega_0)}\right)^{2n+2}, \tag{9}$$

where k_c represents the wave number corresponding to the Compton wavelength at the present epoch. Thus, the $f(R)$ model is specified by n and k_c. The growth factor can be obtained by solving Eq. (7), which we denote by $D_1(a, k)$. The growth rate is given by $f = d\ln D_1(a, k)/d\ln a$.

In the Einstein–de Sitter background universe, the evolution of the density perturbation can be solved analytically [69]. Two of the authors of the present paper investigated characteristic features of the evolution of the growth rate of

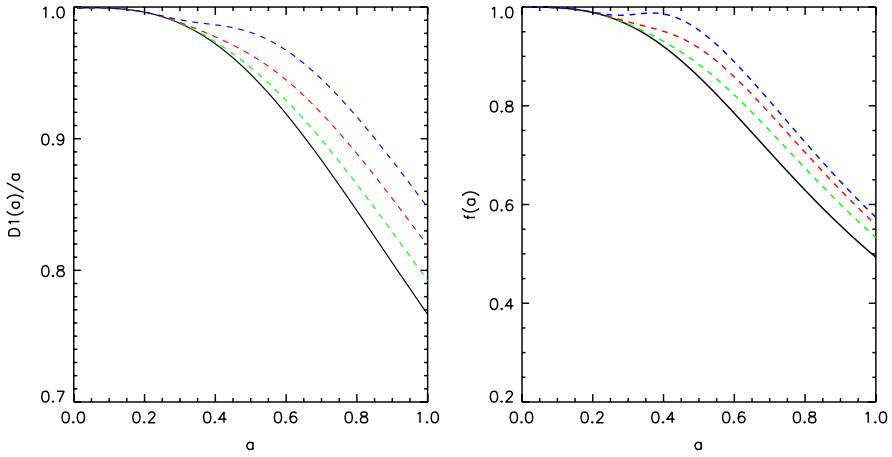

FIG. 1 (color online). (a) $D_1(a)/a$ as a function of the scale factor. The solid curve is the ΛCDM model with $\Omega_0 = 0.28$. The dashed curves are for the $f(R)$ model with the wave numbers $k/(h\ \mathrm{Mpc}^{-1}) = 0.2$, 0.1, and 0.05 from top to bottom, respectively. Here we adopted the model $n = 1$ and $k_c = 0.05h\ \mathrm{Mpc}^{-1}$. (b) Same as (a) but for the growth factor $f = d\ln D_1/d\ln a$.

the $f(R)$ model, both numerically and analytically in Ref. [70]. In the present paper, we solve the evolution equation (7) numerically (cf. [71,72]). Figure 1 shows the growth factor divided by the scale factor (left) and the growth rate (right), respectively, as a function of the scale factor. The solid curve is the ΛCDM model with the density parameter $\Omega_0 = 0.28$. The dashed curves are for the $f(R)$ model with different wave numbers $k/(h\ \mathrm{Mpc}^{-1}) = 0.2$, 0.1, and 0.05, respectively. Here the $f(R)$ model assumes $n = 1$ and $k_c = 0.05h\ \mathrm{Mpc}^{-1}$. Because of the modification of the gravity the growth factor and the growth rate are enhanced, and this enhancement is scale-dependent.

III. MULTIPOLE SPECTRUM OF THE SDSS LRG SAMPLE

The multipole power spectrum $P_\ell(k)$ is defined by the coefficient of the multipole expansion of the anisotropic power spectrum $P(k, \mu)$,

$$P(k, \mu) = \sum_{\ell=0,2,4\ldots} P_\ell(k)\mathcal{L}_\ell(\mu)(2\ell + 1), \qquad (10)$$

where $\mathcal{L}_\ell(\mu)$ are the Legendre polynomials, $\mu(= \cos\theta)$ is the directional cosine between the line of sight direction and the wave number vector $\mathbf{k}$. Note that our definition of the multipole spectrum $P_\ell(k)$ is different from the conventional one by the factor $2\ell + 1$ [35,36,73]. Here the Legendre polynomials satisfy the normalization condition

$$\int_{-1}^{+1} d\mu \mathcal{L}_\ell(\mu)\mathcal{L}_{\ell'}(\mu) = \frac{2}{2\ell + 1}\delta_{\ell\ell'}. \qquad (11)$$

The monopole $P_0(k)$ represents the angular averaged power spectrum, which is what we usually mean by the power spectrum; the quadrupole $P_2(k)$ represents the leading anisotropy in the power spectrum because of the redshift-space distortion. The hexadecapole $P_4(k)$ represents a different aspect of the redshift-space distortion. In the present paper, we focus on the monopole and quadrupole spectra. The quadrupole spectrum reflects the peculiar velocities of the galaxies [35,36,73]. Those peculiar motions can be used to test the gravity theory on cosmological scales.

Pioneering works on the measurement of the quadrupole spectrum was carried out by Cole, Fisher, and Weinberg [35] and Hamilton [36] using the IRAS galaxy survey catalog. Cole *et al.* presented a systematic method to estimate the quadrupole power spectrum through the anisotropic power spectrum [35]. The method was applied to the two degree field (2dF) galaxy survey to estimate the β factor. Hamilton obtained the quadrupole power spectrum by a transformation of the correlation functions [36]. In the present work, however, we adopt a different method to estimate the quadrupole power spectrum [74]. Our method is in line with the widely used way to estimate the monopole power spectrum [75,76], and allows us to obtain the multipoles of the redshift-space power spectrum without evaluating the correlation function or the anisotropic power spectrum. In Ref. [31], we applied the method to the SDSS LRG sample from DR 6 to test the general relativity on cosmological scales. In the present paper, we revisit this problem with the SDSS LRG sample of DR 7 [77].

Our LRG sample is restricted to the redshift range $z =$ 0.16–0.47. In order to reduce the sidelobes of the survey window we remove some noncontiguous parts of the sample (e.g., three southern slices), which leads us to $\sim$7150 $\mathrm{deg}^2(= \Delta\mathcal{A})$ sky coverage with a total of $N =$ 100 157 LRGs. The data reduction procedure is the same as that described in [39]. In this power spectrum analysis, we adopted the spatially flat lambda cold dark matter (ΛCDM) model distance-redshift relation $s = s[z]$, which is consistently chosen when comparing with theoretical prediction.

The strategy to measure the multipole power spectrum is the same as that described in [74]. We adopt the estimator of the multipole power spectrum for the discrete density field of the galaxy catalog, as follows:

$$P_\ell(k) = \frac{1}{\Delta V_k}\int_{\Delta V_k} d^3k(R_\ell(\mathbf{k}) - S_\ell(\mathbf{k})), \tag{12}$$

where ΔV_k is the shell in the Fourier space and

$$R_\ell(\mathbf{k}) = A^{-1}\Big[\sum_{i_1}^{N}\psi(\mathbf{s}_{i_1},\mathbf{k})e^{i\mathbf{k}\cdot\mathbf{s}_{i_1}}\mathcal{L}_\ell(\hat{\mathbf{s}}_{i_1}\cdot\hat{\mathbf{k}}) - \alpha\sum_{j_1}^{N_{\rm rnd}}\psi(\mathbf{s}_{j_1},\mathbf{k})e^{i\mathbf{k}\cdot\mathbf{s}_{j_1}}\mathcal{L}_\ell(\hat{\mathbf{s}}_{j_1}\cdot\hat{\mathbf{k}})\Big] \times\Big[\sum_{i_2}^{N}\psi(\mathbf{s}_{i_2},\mathbf{k})e^{-i\mathbf{k}\cdot\mathbf{s}_{i_2}} - \alpha\sum_{j_2}^{N_{\rm rnd}}\psi(\mathbf{s}_{j_2},\mathbf{k})e^{i\mathbf{k}\cdot\mathbf{s}_{j_2}}\Big], \tag{13}$$

$$S_\ell(\mathbf{k}) = A^{-1}(1+\alpha)\sum_{i_1}^{N}\psi(\mathbf{s}_{i_1},\mathbf{k})\mathcal{L}_\ell(\hat{\mathbf{s}}_{i_1}\cdot\hat{\mathbf{k}}), \tag{14}$$

where $\mathbf{s}_{i_1}$ ($\mathbf{s}_{j_1}$) is the position of galaxies (random sample); ψ is the weight factor, which we take as $\psi = 1$; $\mu = \hat{\mathbf{s}}\cdot\hat{\mathbf{k}}$ is the directional cosine between $\hat{\mathbf{s}}(=\mathbf{s}/|\mathbf{s}|)$ and $\hat{\mathbf{k}}(=\mathbf{k}/|\mathbf{k}|)$; $\alpha \equiv N/N_{\rm rnd}$ and in our case is 0.05; and A is determined by

$$A = \int_{s(z_{\rm min})}^{s(z_{\rm max})} d\mathbf{s}\bar{n}^2(z)\psi^2(\mathbf{s},\mathbf{k}). \tag{15}$$

Here the integral in the expression for A means the integration over the whole survey volume, and $\bar{n}(z)$ is the mean (comoving) number density of the galaxies. The error for the estimator $P_\ell(k)$ is given by the variance [74]

$$\langle\Delta P_\ell(k)^2\rangle \simeq 2\frac{(2\pi)^3}{\Delta V_k}\mathcal{Q}_l^2(k), \tag{16}$$

with

$$\mathcal{Q}_l^2(k) = \frac{1}{\Delta V_k}\int_{\Delta V_k} d\mathbf{k}A^{-2}\int_{s(z_{\rm min})}^{s(z_{\rm max})} d\mathbf{s}\bar{n}^4(z)\psi^4(\mathbf{s},\mathbf{k}) \times[P(\mathbf{k},\mathbf{s}) + 1/\bar{n}(\mathbf{s})]^2\mathcal{L}_\ell^2(\hat{\mathbf{s}}\cdot\hat{\mathbf{k}}). \tag{17}$$

Here we have assumed $\alpha \ll 1$. The covariance between the errors of different multipole spectra $\langle\Delta P_\ell(k)\Delta P_{\ell'}(k)\rangle$ can be evaluated with the same formulas (16) and (17), but only replacing $\mathcal{L}_\ell^2(\hat{\mathbf{s}}\cdot\hat{\mathbf{k}})$ by $\mathcal{L}_\ell(\hat{\mathbf{s}}\cdot\hat{\mathbf{k}})\mathcal{L}_{\ell'}(\hat{\mathbf{s}}\cdot\hat{\mathbf{k}})$ in (17) [78]. In our analysis we adopt $\psi(\mathbf{s},\mathbf{k}) = 1$. Figure 2 shows the mean number density as a function of z, when assuming the ΛCDM with $\Omega_0 = 0.28$ for the distance-redshift relation $s = s[z]$.

Figure 3 compares the observed monopole power spectrum and our theoretical model. The dark (black) points with error bars in Fig. 3 show the monopole power spectrum of the DR 7. The light (green) points are the previous results for the DR 6 [31]. The dashed and the dotted curves represent the $f(R)$ model with $n = 1/2$, with the scale-dependent bias model of case 1 (see the next section for details). The dashed curve is for $k_c = 1h$ Mpc^{-1}, while the dotted one for $10^{-3}h$ Mpc^{-1}. The cosmological parameters are $\Omega_0 = 0.28$, $h = 0.7$, and $n_s = 0.96$ (primordial spectral index). The amplitude of the primordial perturba-

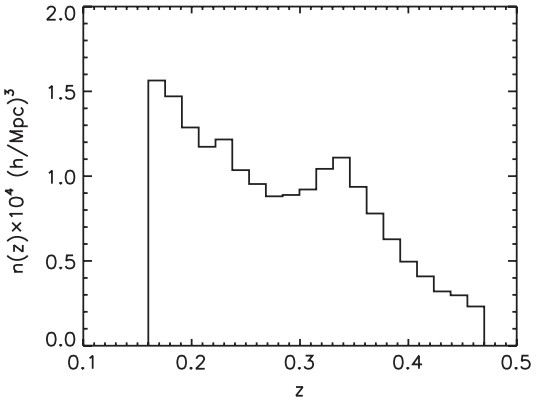

FIG. 2. The mean number density of galaxies $\bar{n}$ as a function of the redshift z of the SDSS LRG sample, where we adopted the ΛCDM model with $\Omega_0 = 0.28$ for the distance-redshift relation $s = s[z]$.

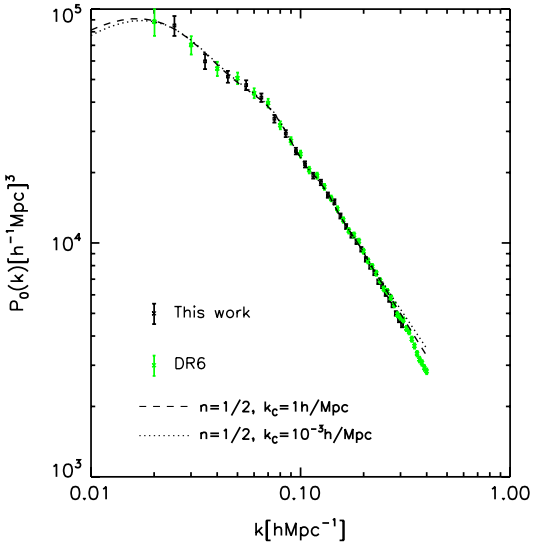

FIG. 3 (color online). $P_0(k)$ of the SDSS LRG sample, where we adopted the distance-redshift relation $s = s[z]$ of the ΛCDM model with $\Omega_0 = 0.28$. The dark (black) points correspond to the DR 7, while the light (green) ones to the DR 6. The dashed and dotted curves show the $f(R)$ model with $n = 1/2$, adopting a scale-dependent bias [case 1 in Eq. (23)] and $\sigma_{\rm v} = 350$ km/s. The dashed curve is for $k_c = 1h$ Mpc^{-1}, while the dotted curve is $k_c = 10^{-3}h$ Mpc^{-1}. The cosmological parameters are $\Omega_0 = 0.28$, $h = 0.7$, and $n_s = 0.96$ (primordial spectral index), and the amplitude of the perturbation is determined so as to be $\sigma_8 = 0.8$ in the limit of infinitely large k_c.

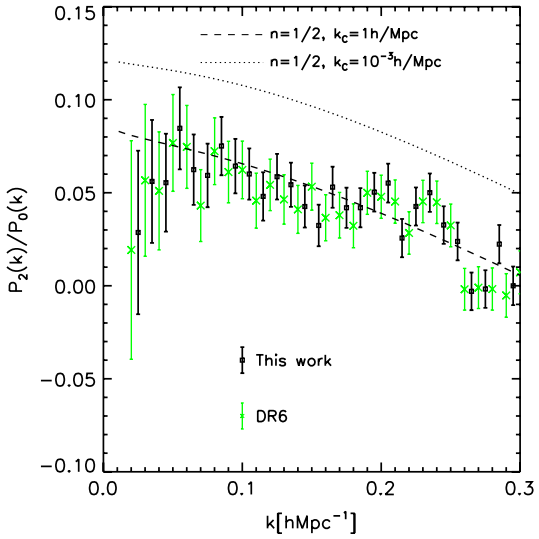

FIG. 4 (color online). $P_2(k)/P_0(k)$ of the SDSS LRG sample. The meaning of the points corresponds to those of Fig. 3. The dashed (dotted) curve is the theoretical prediction of the $f(R)$ model with $n = 1/2$, $k_c = 1h$ Mpc^{-1} ($10^{-3}h$ Mpc^{-1}). The parameters of the bias model and σ_v are the same as those of Fig. 3. The other cosmological parameters and the amplitude of the primordial perturbation of the $f(R)$ model are also the same as those of Fig. 3.

tion is chosen to be $\sigma_8 = 0.8$ in the limit of infinitely large k_c. The Smith nonlinear fitting formula [79] is adopted. One can see that $P_0(k)$ can be fitted with our theoretical model by choosing suitable bias parameters.

Figure 4 plots $P_2(k)/P_0(k)$. The meaning of the points and the parameters of the curves corresponds to those of Fig. 3. This figure shows that the quadrupole power spectrum can be used to constrain the $f(R)$ model. Also it is clear that the long Compton wavelength model does not fit the data.

IV. COSMOLOGICAL CONSTRAINT

In order to investigate the cosmological constraint on the $f(R)$ model from the multipole spectra, our theoretical model needs to include nonlinear effects. In the present paper, for simplicity, we adopt the following model for the galaxy power spectrum [80,81],

$$P_{\rm gal}(k, \mu, z) = (b + f\mu^2)^2 P_{\rm nl}(k, z)\mathcal{D}[\sigma_v k\mu], \tag{18}$$

where $P_{\rm nl}(k, z)$ denotes a nonlinear matter power spectrum, $\mathcal{D}[k\mu\sigma_v]$ is the damping factor due to the finger of God effect, and σ_v^2 is the pairwise velocity dispersion. Assuming an exponential distribution function for the pairwise velocity, $e^{-\sqrt{2}|v_{12}|/\sigma_v}/\sqrt{2}\sigma_v$, where v_{12} is the pairwise peculiar velocity projected along the separation of a pair, the damping function is [82] (cf. [83,84])

$$\mathcal{D}[\sigma_v k\mu] = \frac{1}{1 + \tilde{\sigma}_v^2 k^2\mu^2/2}, \tag{19}$$

with $\tilde{\sigma}_v = \sigma_v/H_0$. In this case, we have

$$P_0(k, z) = \frac{1}{3k^5\tilde{\sigma}_v^5}\Big[2fk\tilde{\sigma}_v(-6f + (6b + f)k^2\tilde{\sigma}_v^2) + 3\sqrt{2}(-2f + bk^2\tilde{\sigma}_v^2)^2\tan^{-1}\frac{k\tilde{\sigma}_v}{\sqrt{2}}\Big]P_{\rm nl}(k, z), \tag{20}$$

$$P_2(k, z) = \frac{1}{30k^7\tilde{\sigma}_v^7}\Big[-360bfk^3\tilde{\sigma}_v^3 + 90b^2k^5\tilde{\sigma}_v^5 + 8f^2k\tilde{\sigma}_v(45 + k^4\tilde{\sigma}_v^4) - 15\sqrt{2}(6 + k^2\tilde{\sigma}_v^2) \times (-2f + bk^2\tilde{\sigma}_v^2)^2\tan^{-1}\frac{k\tilde{\sigma}_v}{\sqrt{2}}\Big]P_{\rm nl}(k, z), \tag{21}$$

$$P_4(k, z) = \frac{(-2f + bk^2\tilde{\sigma}_v^2)^2}{24k^9\tilde{\sigma}_v^9}\Big[-10k\tilde{\sigma}_v(42 + 11k^2\tilde{\sigma}_v^2) + 3\sqrt{2}(140 + 60k^2\tilde{\sigma}_v^2 + 3k^4\tilde{\sigma}_v^4)\tan^{-1}\frac{k\tilde{\sigma}_v}{\sqrt{2}}\Big] \times P_{\rm nl}(k, z), \tag{22}$$

from Eqs. (18) and (19). For the nonlinear matter power spectrum $P_{\rm nl}(k, z)$, we adopt the fitting formulas by Peacock and Dodds [85] or by Smith *et al.* [79]. For the bias, we consider the following scale-dependent forms,

$$b(k) = \begin{cases} b_0 + b_1(\frac{k}{0.1h\ \rm Mpc^{-1}})^\alpha & \text{case 1} \\ b_0 + b_1(\frac{k}{0.1h\ \rm Mpc^{-1}}) + b_2(\frac{k}{0.1h\ \rm Mpc^{-1}})^2 & \text{case 2'} \end{cases} \tag{23}$$

where b_0, b_1, b_2, and α are the fitting parameters.

Our strategy is the following. We use the monopole and quadrupole spectra in the wave number range $0.02h$ Mpc$^{-1} \le k_i \le 0.2h$ Mpc^{-1}, and compute the chi squared

$$\chi^2 = \sum_{\ell,\ell'=0,2}\sum_{i,j}(P_\ell(k_i) - P_\ell^{\rm obs}(k_i))C_{\ell\ell'}^{-1}(k_i, k_j) \times (P_{\ell'}(k_j) - P_{\ell'}^{\rm obs}(k_j)), \tag{24}$$

where $P_\ell^{\rm obs}(k_i)$ is the observed power spectrum and $C_{\ell\ell'}(k_i, k_j) = \langle\Delta P_\ell(k_i)\Delta P_{\ell'}(k_j)\rangle$ is the covariance matrix. Here the covariance of the errors of the monopole and quadrupole spectra is taken into account, however, it does not affect our results quantitatively.

The left panel of Fig. 5 shows the contours of $\Delta\chi^2$ on the $k_c - \sigma_v$ plane, where we used the covariance matrix from Sec. III,

$$C_{\ell\ell'}(k_i, k_j) = \langle\Delta P_\ell(k_i)\Delta P_{\ell'}(k_j)\rangle\delta_{ij}. \tag{25}$$

The one-sigma (dashed curve) and two-sigma (solid curve) contour levels are given, respectively. Here the chi squared is computed to minimize (24) by fitting the bias parameters

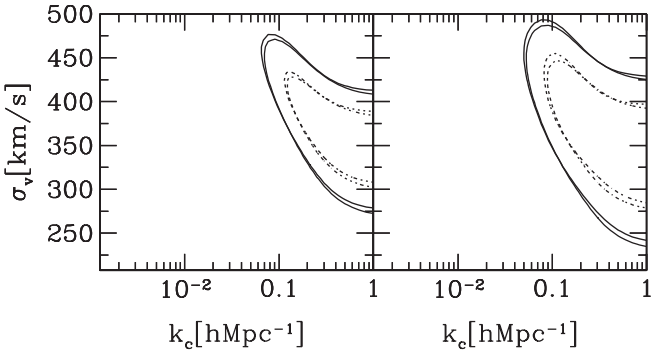

FIG. 5. $\Delta\chi^2$ on the $k_c - \sigma_v$ plane. Here we adopted the model $n = 1/2$. The other parameters are $\Omega_0 = 0.28$, $h = 0.7$, and $n_s = 0.96$. The normalization is fixed $\sigma_8 = 0.8$ in the limit of large k_c. The Peacock and Dodds nonlinear fitting formula is used for the thin curves, while the Smith formula is used for the thick curves. Solid (dashed) contours correspond to $\Delta\chi^2 = 6.2$ ($\Delta\chi^2 = 2.3$). The left panel adopted Eq. (25), while the right panel used the covariance matrix from the mock catalogs.

b_0, b_1, b_2, or α, for each value of k_c and σ_v. The other parameters are fixed $n = 1/2$, $\Omega_0 = 0.28$, $\Omega_b = 0.044$, $n_s = 0.96$, and $h = 0.7$. For $P_{nl}(k, z)$, we adopted the Peacock and Dodds formula [85] (thin curve) and the Smith formula [79] (thick curve), respectively. The redshift is fixed to $z = 0.3$, which is typical for the LRG sample. The amplitude of the matter power spectrum is fixed so as to be $\sigma_8 = 0.8$ in the limit of infinitely large k_c, i.e., in the limit of the ΛCDM model.

For comparison, the right panel of Fig. 5 shows the contours of $\Delta\chi^2$, which take the correlation of the errors of different wave numbers into account by evaluating Eq. (24), with the covariance matrix obtained from mock catalogs. Because of the inclusion of the correlation of errors of different wave numbers, the constraint becomes weaker compared with the left panel.

In the right panel of Fig. 5, we obtain the covariance matrix by using mock catalogs, which were built by following the procedure described in Ref. [39]. First, we generate the density field using a second order Lagrangian perturbation calculation. Then, we perform Poisson sampling of the generated density field so as to end up with a galaxy sample that has a clustering strength enhanced by a bias and a number density equal to the observed LRG sample density. We then extract the catalog by applying the radial and angular selection function. We have checked that the mock catalogs have the amplitude of the monopole and quadrupole power spectra consistent with the observed LRG power spectra, and also that the diagonal components of the covariance matrix from the mock catalogs give almost the same error as those of Eq. (16) in the range of $0.02h$ Mpc$^{-1} \le k_i \le 0.2h$ Mpc^{-1} [39,86]. Figure 6 shows the two-dimensional map of the correlation matrix

$$r_\ell(k_i, k_j) = \frac{C_{\ell\ell}(k_i, k_j)}{\sqrt{C_{\ell\ell}(k_i, k_i) C_{\ell\ell}(k_j, k_j)}}, \tag{26}$$

for $\ell = 0$ and 2 from 1000 mock catalogs. The binning of the covariance matrix is $\Delta k = 0.01h$ Mpc^{-1}. One can see from Fig. 6 that the off-diagonal part is suppressed.

The normalization of the cosmological perturbations should be determined by the cosmic microwave background anisotropies, depending on the parameters n and k_c of the $f(R)$ model. However, the background expansion of the viable $f(R)$ model is almost the same as that of the ΛCDM model, and the evolution of the matter density perturbations is only altered at late time, if compared with the ΛCDM model. This alteration will raise an additional integrated Sachs-Wolfe effect on the CMB anisotropies due to the modified evolution of the matter density perturbation at late time. We neglect this effect on the normalization of the perturbation, for simplicity. Then,

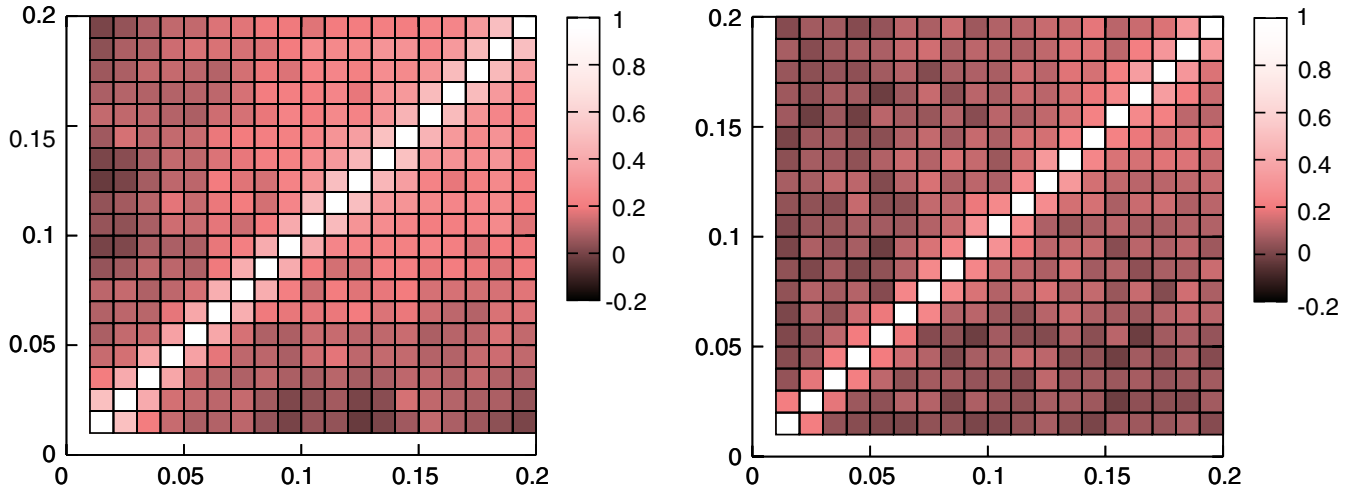

FIG. 6 (color online). The correlation matrix, Eq. (26), for $\ell = 0$ (left) and $\ell = 2$ (right), respectively, from 1000 mock catalogs.

we simply fixed the amplitude of the primordial cosmological perturbation by σ_8 in the limit of large k_c, i.e., the σ_8 of the ΛCDM model.

Figure 5 shows that the shorter Compton wavelength model with $\sigma_v \simeq 350$ km/s gives the best fit to the data. Figure 7 shows the contours of $\Delta\chi^2$ on the $k_c - n$ plane. Here χ^2 is computed with Eq. (24) with (25) by fitting the bias parameters and σ_v. Figures 7(a)–7(c)fix the normalization of the perturbation to be $\sigma_8 = 0.8$, 0.82, and 0.78, in the limit of large k_c, respectively. The contour levels of $\Delta\chi^2 = 2.3$ (dotted curve) and 6.2 (solid curve) correspond to 1σ and 2σ confidence, respectively. In Fig. 7 we used the Peacock and Dodds formula (thin curve) and the Smith formula [79] (thick curve), respectively, though the two curves almost overlap. Figures 7(a)–7(c) adopt the bias model of case 1. Figure 7(d) is the same as Fig. 7(a), but adopted the bias model of case 2. The left lower region in each panel is excluded.

Figure 8 is the same as Fig. 7, but adopted the covariance matrix from the mock catalogs for the chi squared. The constraint of Fig. 8 is weaker compared with that of Fig. 7. Especially, the constraint for the model with larger n becomes weaker. However, Fig. 8 indicates that the long

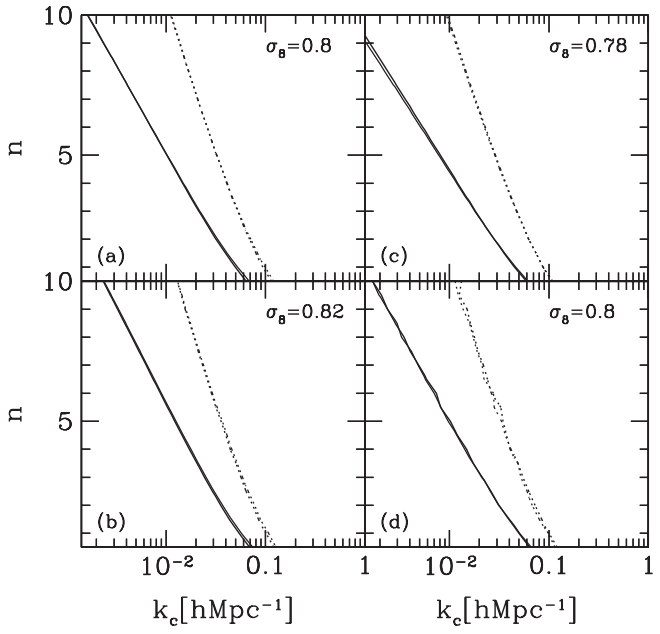

FIG. 7. $\Delta\chi^2$ on the $k_c - n$ plane, which we evaluated with Eqs. (24) and (25). For each pair of k_c and n, the minimum value of χ^2 is computed by fitting the bias parameter and σ_v. Other parameters are fixed: $\Omega_0 = 0.28$, $h = 0.7$, and $n_s = 0.96$. The normalization of the primordial perturbation is chosen so as to be $\sigma_8 = 0.8$ (a), $\sigma_8 = 0.82$ (b), and $\sigma_8 = 0.78$ (c), in the limit of large k_c. The panels (a)–(c) adopt the bias model of case 1. Panel (d) is the same as (a) but with bias model of case 2. Solid (dotted) contours correspond to $\Delta\chi^2 = 6.2$ (2.3). Almost overlapping thin and thick curves assume Peacock and Dodds's formula and Smith's formula, respectively.

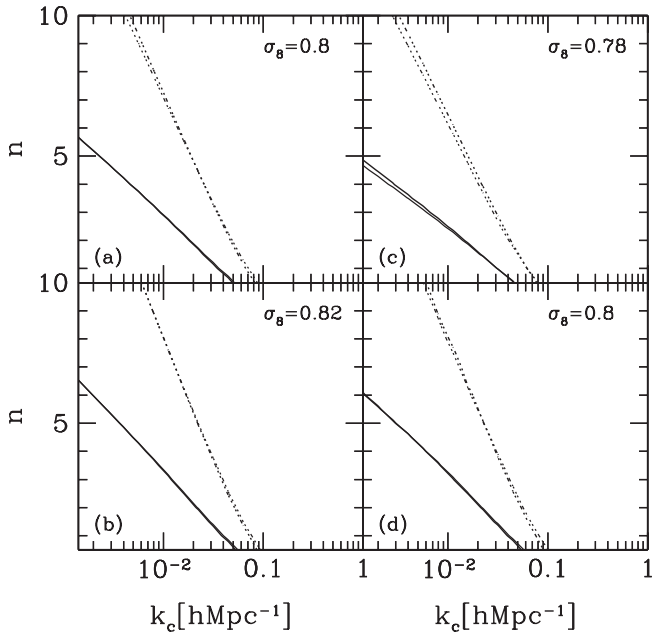

FIG. 8. The same as the Fig. 7 but with the covariance matrix from the mock catalogs.

Compton wavelength case of the $f(R)$ model with the smaller value of n is excluded.

Thus far, we have used the redshift-space power spectrum (18). In order to check the reliability of our result, we next consider the other possible model for the redshift-space power spectrum,

$$P_g(k,\mu) = (b^2(k)P_{\delta\delta}(k) + 2fb(k)P_{\delta\theta}(k)\mu^2 + f^2P_{\theta\theta}(k)\mu^4)e^{-(fk\mu\sigma_v)^2}, \quad (27)$$

where $P_{\delta\delta}(k)$ is the nonlinear matter power spectrum, $P_{\theta\theta}(k)$ is the power spectrum of the velocity divergence, and $P_{\delta\theta}(k)$ is the cross power spectrum of matter and the velocity divergence. This model is obtained from the model proposed by Scoccimarro [87] and assumes a linear bias relation. Very recently, Jenning *et al.* proposed a fitting formula for the redshift-space power spectrum of the form (27), assuming $b(k) = 1$. The fitting formula relates the nonlinear matter power spectrum $P_{\delta\delta}(k)$ to $P_{\delta\theta}(k)$ and $P_{\theta\theta}(k)$. By using the N-body simulations it was demonstrated that the fitting formula is accurate to better than 10% for the ΛCDM model and quintessence dark energy models for $k \lesssim 0.2h$ Mpc^{-1}. Although the accuracy of the fitting formula for the $f(R)$ model has not been explicitly demonstrated, we assume its validity, and use it in the following $\Delta\chi^2$ calculations.

Figure 9 shows the contours of $\Delta\chi^2$ on the $k_c - n$ plane, the same as Fig. 7, but with the covariance matrix from the mock catalogs and the redshift-space power spectrum (27). In the original formula, σ_v is obtained from $P_{\theta\theta}(k)$, however, we assumed σ_v to be a fitting parameter, as is done in Fig. 8. This figure shows that the constraint becomes

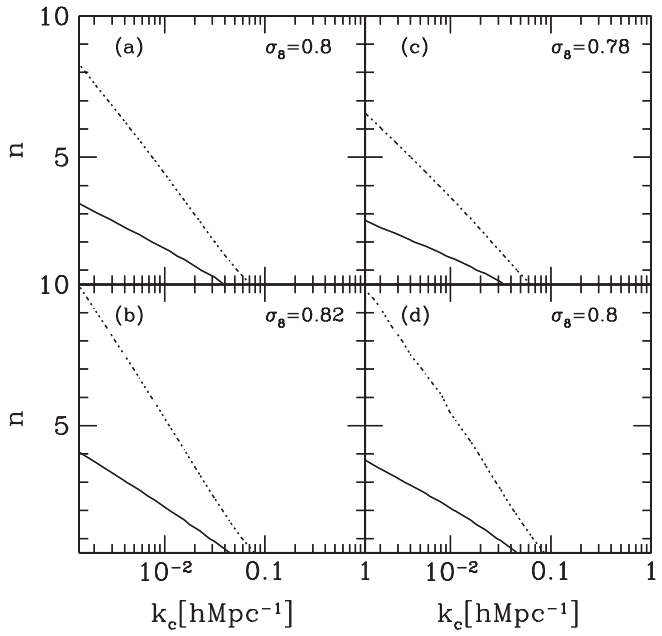

FIG. 9. The same as the Fig. 7 but with the covariance matrix from the mock catalogs and the redshift-space power spectrum (27). Only the curves with Peacock and Dodds's formula for the nonlinear matter power spectrum are plotted.

weaker when compared to the previous model (18). The models with large values of n are not constrained. However, the long Compton wavelength case of the $f(R)$ model with the smaller value of n is excluded. This new model predicts that $P_{\delta\theta}(k)$ is smaller than $P_{\delta\delta}(k)$ for values of $k \lesssim 0.1$ Mpc^{-1}, which reduces the quadrupole power spectrum and thus weakens the constraint.

Let us compare our result with the other constraints on the $f(R)$ model. References [56,57] have investigated the constraints on the $f(R)$ model for the case $n = 1/2$. In Ref. [56], the constraint from the CMB anisotropies through the integrated Sachs-Wolfe effect is investigated. However, the constraint is weak. Only the horizon-scale Compton wavelength model is excluded. In Ref. [57], the constraint from the cluster number count is investigated. Though it is restricted to the case $n = 1/2$, they obtained $|f_{R0}| \lesssim 10^{-4}$, where f_{R0} is the value of f_R at the present epoch. In the case $n = 1/2$, $|f_{R0}|$ is related to k_c by

$$k_c \simeq 0.04\left(\frac{10^{-4}}{|f_{R0}|}\right)^{1/2} h \text{ Mpc}^{-1}. \tag{28}$$

Reference [57] reports that $k_c \lesssim 0.04h$ Mpc^{-1} is excluded. The constraint is similar to our result, when the redshift-space power spectrum (18) is used (see Fig. 8). When an arguably more accurate model (27) is used, the constraint becomes slightly weaker than that of (18) (see Fig. 9).

V. FUTURE PROSPECT OF MEASURING COMPTON SCALE

In this section, we estimate future prospects of constraining the Compton scale with the use of the Fisher matrix technique, which is frequently used for estimating minimal attainable constraint on model parameters. We focus on the error of the Compton wave number k_c. We adopt the Fisher matrix of the form (e.g., [88])

$$F_{ij} = \frac{1}{4\pi^2}\int_{k_{\min}}^{k_{\max}} dk k^2 \int_{-1}^{+1} d\mu \frac{\partial P_{\rm gal}(k,\mu)}{\partial\theta^i}\frac{\partial P_{\rm gal}(k,\mu)}{\partial\theta^j} \times \frac{V}{(P_{\rm gal}(k,\mu)+1/\bar{n})^2}, \tag{29}$$

where θ^i denotes a model parameter, V is a survey volume, $\bar{n}$ is a mean number density of galaxies.

In the Fisher matrix analysis, for simplicity, we consider the 6 parameters k_c, n, σ_v, b_0, b_1, and α, adopting the bias model of case 1. Figure. 10(a) shows the 1σ error Δk_c, in determining the Compton wave number k_c as a function of the target value of k_c, assuming a redshift survey like the

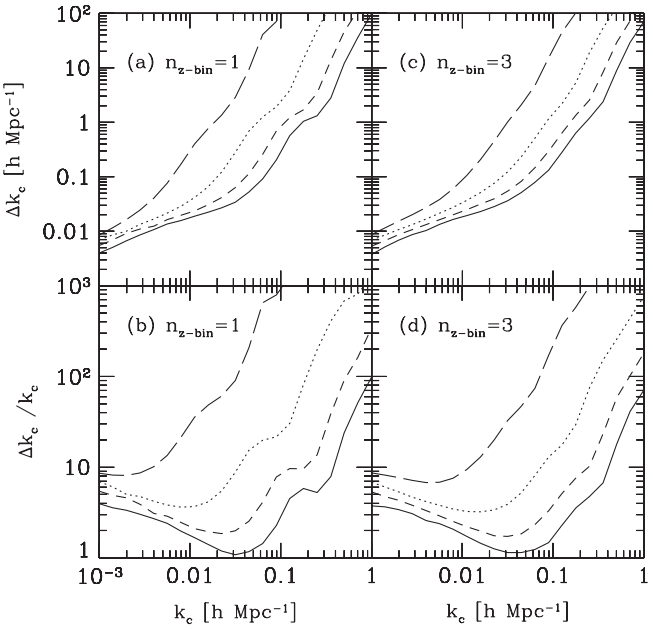

FIG. 10. (a) 1σ error Δk_c as a function of the target value of k_c. The result is based on the Fisher matrix analysis with the 6 parameters, k_c, n, σ_v, and b_0, b_1, and α for the bias model 1, and marginalized over the 5 parameters other than k_c. The target parameters are $b_0 = 2.5$, $b_1 = 0.5$, $\alpha = 1/2$, and n is chosen $n = 1/2, 1, 2, 4$ from bottom to top, respectively. The other parameters are fixed $\Omega_0 = 0.28$, $h = 0.7$, $n_s = 0.96$, and the normalization $\sigma_8 = 0.8$ in the limit of the ΛCDM model. Equation (18) with the Peacock and Dodds nonlinear fitting formula is adopted. (b) The relative error $\Delta k_c/k_c$ corresponding to (a). (c) and (d) are the same as (a) and (b), respectively, but assumed the analysis where the full sample is divided into 3 redshift bins.

SUMIRE (Subaru measurement of imaging and redshift of the Universe) [9], which assumes the survey parameters like those of the wide-field multiobject spectrograph (WFMOS) survey [89], the range of the redshift $0.9 < z < 1.6$, the survey area 2000 square degrees, and the mean number density $\bar{n} = 4 \times 10^{-4} (h^{-1}\ \mathrm{Mpc})^{-3}$. Here we adopted the target values $\sigma_v = 400$ km/s, $b_0 = 2.5$, $b_1 = 0.5$, $\alpha = 0.5$, and $n = 1/2$, 1, 2, and 4, from the bottom to the top, respectively. The other parameters are fixed: $\Omega_0 = 0.28$, $h = 0.7$, $n_s = 0.96$, and the normalization so as to be $\sigma_8 = 0.8$ in the limit of the ΛCDM model. We obtained Δk_c by marginalizing the Fisher matrix over the 5 parameters n, σ_v, b_0, b_1 and α. Figure 10(b) shows the relative error $\Delta k_c / k_c$.

In the Fisher matrix we used the power spectrum in the range of wave numbers $k < 0.3h\ \mathrm{Mpc}^{-1}$. This immediately implies that the redshift survey cannot be very sensitive to the models with the short Compton wavelength, as seen from Fig. 10. The error becomes very large for $k_c \gtrsim 0.1h\ \mathrm{Mpc}^{-1}$, but it will be possible to obtain a useful constraint on the Compton scale, in principle, for models with $k_c \lesssim 0.1h\ \mathrm{Mpc}^{-1}$. However, the constraint becomes weak for the case of large n.

Figure 10(a) assumes the power spectrum analysis without dividing the full galaxy sample, which spans the redshift range $0.9 \leq z \leq 1.6$, into redshift subsamples. Figure 10(c) assumes the case when the galaxy sample is divided into the three subsamples in redshift bins and that the power spectra are obtained from each subsample. In this case, the parameters σ_v, b_0, b_1, and α should be fitted in each redshift bin, and the total number of parameters in the Fisher matrix analysis is 14. Figure 10(d) is the relative error, corresponding to 10(c). The cosmological parameters are the same as those of 10(a). The possible advantage of this method is that the additional information of the redshift evolution might improve the constraint. One can see that the constraint is improved in comparison with Figs. 10(a) or 10(b). The degree of the improvement is small for $n = 1/2$, but is not negligible for the case $n = 4$. This is understood because the redshift evolution of the Compton scale is faster for larger n.

VI. SUMMARY AND CONCLUSIONS

In this paper, we determined a cosmological constraint on the viable $f(R)$ model based on the redshift-space distortion by measuring the monopole and quadrupole spectra of the SDSS LRG sample of DR 7. The monopole and the quadrupole spectra are used to fit the bias parameters and to constrain the growth factor and the growth rate of the density perturbations, which depend on the Compton scale of the $f(R)$ model.

Our results show that the short Compton wavelength model fits the data better, while the long Compton wavelength model is excluded, though the constraint depends on the evolution parameter n. For the case $n = 1/2$, our constraint is similar to that from the cluster number counts reported in [57]. When we adopt a more accurate model for the redshift-space power spectrum [90], the constraint becomes slightly weaker. However, the long Compton wavelength case of the $f(R)$ model with the smaller value of n is excluded. Our results exemplify that the redshift-space distortion is quite useful in testing gravity theory. We also demonstrated that a future redshift survey like the WFMOS/SUMIRE is potentially useful in obtaining a constraint on the Compton wavelength scale.

We acknowledge that the widely used theoretical model of the anisotropic power spectrum adopted in the present paper might need careful improvements. We adopted the Peacock and Dodds formula and the Smith formula for the nonlinear modeling of the mass power spectrum. Our results do not significantly depend on the choice. However, there might be a need to adopt a more sophisticated formula for the precise nonlinear modeling within the framework of the modified gravity, as demonstrated by Koyama, Taruya, and Hiramatsu [91]. The treatment of the finger of God effect in our paper was simple, which assumed the exponential distribution function for the pairwise velocity and introduced one free parameter—the pairwise velocity dispersion. In reality it might not be an adequate model to describe the nonlinear region of the redshift-space power spectrum [87]. We checked the reliability of our results by adopting the other possible model proposed in Ref. [90], extensively applying the fitting formula to the $f(R)$ model, whose accuracy in this case, however, has not been demonstrated. We found that there is a non-negligible effect on the constraint on the $f(R)$ model. Therefore, a more precise modeling of the redshift-space power spectrum should arguably be needed in the future. Concerning the modeling of the clustering bias, we adopted a simple scale-dependent bias. Here too there is potentially a lot of room for improvement. These issues are outside the scope of the present paper, but need to be elaborated for a precise test of gravity with the future redshift surveys.

ACKNOWLEDGMENTS

We thank T. Kobayashi, J. Yokoyama, H. Motohashi, T. Nishimichi, S. Saito, A. Taruya and M. Takada, and Y. Suto for useful comments and discussions. This work was supported by Japan Society for Promotion of Science (JSPS) Grants-in-Aid for Scientific Research (Nos. 21540270, 21244033). This work was also supported by JSPS Core-to-Core Program "International Research Network for Dark Energy." T. N. acknowledges support by a research assistant program of Hiroshima University.

[1] E. G. Adelberger, B. R. Heckel, and A. E. Nelson, Annu. Rev. Nucl. Part. Sci. **53**, 77 (2003).
[2] A. G. Riess *et al.*, Astron. J. **116**, 1009 (1998).
[3] S. Perlmutter *et al.*, Astrophys. J. **517**, 565 (1999).
[4] D. N. Spergel *et al.*, Astrophys. J. Suppl. Ser. **170**, 377 (2007).
[5] S. Weinberg, Rev. Mod. Phys. **61**, 1 (1989).
[6] P. J. E. Peebles and B. Ratra, Rev. Mod. Phys. **75**, 559 (2003).
[7] A. Albrecht *et al.*, arXiv:astro-ph/0609591.
[8] Sloan Digital Sky Survey III, http://www.sdss3.org/.
[9] H. Aihara, talk at the IPMU International Conference on Dark Energy: Lighting Up the Darkness, Kashiwa, Japan, 2009 (unpublished).
[10] Large Synoptic Survey Telescope, http://www.lsst.org/.
[11] Square Kilometer Array, http://www.skatelescope.org/.
[12] M. Robberto *et al.*, Nuovo Cimento Soc. Ital. Fis. B **122**, 1467 (2007).
[13] K. Yamamoto, B. A. Bassett, R. C. Nichol, Y. Suto, and K. Yahata, Phys. Rev. D **74**, 063525 (2006).
[14] J.-P. Uzan and F. Bernardeau, Phys. Rev. D **64**, 083004 (2001).
[15] A. Shirata *et al.*, Phys. Rev. D **71**, 064030 (2005).
[16] C. Sealfon, L. Verde, and R. Jimenez, Phys. Rev. D **71**, 083004 (2005).
[17] E. V. Linder, Phys. Rev. D **72**, 043529 (2005).
[18] M. Ishak, A. Upadhye, and D. N. Spergel, Phys. Rev. D **74**, 043513 (2006).
[19] J.-P. Uzan, Gen. Relativ. Gravit. **39**, 307 (2007).
[20] E. V. Linder and R. N. Cahn, Astropart. Phys. **28**, 481 (2007).
[21] K. Yamamoto, D. Parkinson, T. Hamana, R. C. Nichol, and Y. Suto, Phys. Rev. D **76**, 023504 (2007).
[22] D. Huterer and E. V. Linder, Phys. Rev. D **75**, 023519 (2007).
[23] M. Kunz and D. Sapone, Phys. Rev. Lett. **98**, 121301 (2007).
[24] V. Acquaviva, A. Hajian, D. N. Spergel, and S. Das, Phys. Rev. D **78**, 043514 (2008).
[25] Y.-S. Song and K. Koyama, J. Cosmol. Astropart. Phys. 01 (2009) 048.
[26] E. Calabrese *et al.*, Phys. Rev. D **77**, 123531 (2008).
[27] J. Guzik, B. Jain, and M. Takada, arXiv:0906.2221.
[28] R. Bean, arXiv:0909.3853.
[29] E. V. Linder, Astropart. Phys. **29**, 336 (2008).
[30] L. Guzzo *et al.*, Nature (London) **451**, 541 (2008).
[31] K. Yamamoto, T. Sato, and G. Hütsi, Prog. Theor. Phys. **120**, 609 (2008).
[32] M. White, Y.-S. Song, and W. J. Percival, Mon. Not. R. Astron. Soc. **397**, 1348 (2009).
[33] F. Simpson and J. A. Peacock, Phys. Rev. D **81**, 043512 (2010).
[34] R. Reyes *et al.*, Nature (London) **464**, 256 (2010).
[35] S. Cole, K. B. Fisher, and D. H. Weinberg, Mon. Not. R. Astron. Soc. **267**, 785 (1994).
[36] A. J. S. Hamilton, in *The Evolving Universe: Selected Topics on Large-Scale Structure and on the Properties of Galaxies, Proceedings of the Ringberg Workshop on Large-Scale Structure, Schloss Ringberg, 1996* (Kluwer, New York, 1998).
[37] K. Yamamoto, B. A. Bassett, and H. Nishioka, Phys. Rev. Lett. **94**, 051301 (2005).
[38] D. J. Eisenstein *et al.*, Astrophys. J. **633**, 560 (2005).
[39] G. Hütsi, Astron. Astrophys. **449**, 891 (2006).
[40] W. J. Percival *et al.*, Astrophys. J. **657**, 645 (2007).
[41] W. J. Percival *et al.*, Astrophys. J. **657**, 51 (2007).
[42] M. Tegmark *et al.*, Phys. Rev. D **74**, 123507 (2006).
[43] G. Hütsi, Astron. Astrophys. **459**, 375 (2006).
[44] W. J. Percival *et al.*, Mon. Not. R. Astron. Soc. **381**, 1053 (2007).
[45] T. Okumura *et al.*, Astrophys. J. **676**, 889 (2008).
[46] A. Cabre and E. Gaztanaga, Mon. Not. R. Astron. Soc. **393**, 1183 (2009).
[47] A. G. Sanchez *et al.*, arXiv:0901.2570 [Mon. Not. R. Astron. Soc. (to be published)].
[48] W. J. Percival *et al.*, Mon. Not. R. Astron. Soc. **401**, 2148 (2010).
[49] B. A. Reid *et al.*, arXiv:0907.1659.
[50] W. Hu and I. Sawicki, Phys. Rev. D **76**, 064004 (2007).
[51] A. A. Starobinsky, JETP Lett. **86**, 157 (2007).
[52] S. Tsujikawa, Phys. Rev. D **77**, 023507 (2008).
[53] S. Nojiri and S. Odintsov, Phys. Lett. B **657**, 238 (2007); Phys. Rev. D **77**, 026007 (2008); G. Cognola *et al.*, Phys. Rev. D **77**, 046009 (2008).
[54] J. Khoury and A. Weltman, Phys. Rev. D **69**, 044026 (2004).
[55] D. F. Mota and J. D. Barrow, Phys. Lett. B **581**, 141 (2004).
[56] Y.-S. Song, H. Peiris, and W. Hu, Phys. Rev. D **76**, 063517 (2007).
[57] F. Schmidt, A. Vikhlinin, and W. Hu, Phys. Rev. D **80**, 083505 (2009).
[58] After we completed this manuscript, we noticed the paper by Girones *et al.* [59], in which the similar cosmological constraint on the $f(R)$ model is investigated.
[59] Z. Girones *et al.*, arXiv:0912.5474.
[60] T. P. Sotiriou and V. Faraoni, Rev. Mod. Phys. 82, 451 (2010).
[61] A. De Felice and S. Tsujikawa, arXiv:1002.4928.
[62] S. Carloni, E. Elizalde, and S. Odintsov, arXiv:0907.3941.
[63] T. Kobayashi and K. I. Maeda, Phys. Rev. D **78**, 064019 (2008).
[64] K. Koyama, A. Taruya, and T. Hiramatsu, Phys. Rev. D **79**, 123512 (2009).
[65] H. Oyaizu, Phys. Rev. D **78**, 123523 (2008).
[66] H. Oyaizu, M. Lima, and W. Hu, Phys. Rev. D **78**, 123524 (2008).
[67] F. Schmidt, M. Lima, H. Oyaizu, and W. Hu, Phys. Rev. D **79**, 083518 (2009).
[68] A. Silvestri and M. Trodden, Rep. Prog. Phys. **72**, 096901 (2009).
[69] H. Motohashi, A. A. Starobinsky, and J. Yokoyama, Int. J. Mod. Phys. D **18**, 1731 (2009).
[70] T. Narikawa and K. Yamamoto, Phys. Rev. D **81**, 043528 (2010).
[71] H. Motohashi, A. A. Starobinsky, and J. Yokoyama, arXiv:1002.0462.
[72] H. Motohashi, A. A. Starobinsky, and J. Yokoyama, arXiv:1002.1141.
[73] N. Kaiser, Mon. Not. R. Astron. Soc. **227**, 1 (1987).
[74] K. Yamamoto, M. Nakamichi, A. Kamino, B. A. Bassett,

and H. Nishioka, Publ. Astron. Soc. Jpn. **58**, 93 (2006).
[75] H. A. Feldman, N. Kaiser, and J. A. Peacock, Astrophys. J. **426**, 23 (1994).
[76] K. Yamamoto, Astrophys. J. **595**, 577 (2003).
[77] K. N. Abazajian *et al.* (SDSS Collaboration), Astrophys. J. Suppl. Ser. **182**, 543 (2009).
[78] The contribution of the covariance between different multipoles was pointed out by Atsushi Taruya and Masahiro Takada.
[79] R. E. Smith *et al.*, Mon. Not. R. Astron. Soc. **341**, 1311 (2003).
[80] J. A. Peacock and S. J. Dodds, Mon. Not. R. Astron. Soc. **267**, 1020 (1994).
[81] S. Cole, K. B. Fisher, and D. H. Weinberg, Mon. Not. R. Astron. Soc. **275**, 515 (1995).
[82] H. Magira, Y. P. Jing, and Y. Suto, Astrophys. J. **528**, 30 (2000).
[83] P. J. E. Peebles, Astrophys. Space Sci. **45**, 3 (1976).
[84] C. Park, M. S. Vogeley, M. J. Geller, and J. Juchra, Astrophys. J. **431**, 569 (1994).
[85] J. A. Peacock and S. J. Dodds, Mon. Not. R. Astron. Soc. **280**, L19 (1996).
[86] T. Sato, G. Hütsi, G. Nakamura, and K. Yamamoto (unpublished).
[87] R. Scoccimarro, Phys. Rev. D **70**, 083007 (2004).
[88] L. Verde, Lect. Notes Phys. **800**, 147 (2010).
[89] B. Bassett, R. C. Nichol, and D. J. Eisenstein, Astron. Geophys. **46**, 5.26 (2005).
[90] E. Jennings, C. M. Baugh, and S. Pascoli, arXiv: 1003.4282.
[91] K. Koyama, A. Taruya, and T. Hiramatsu, Phys. Rev. D **79**, 123512 (2009).